Electrospun iron- and copper oxide fibres for virus retention applications

Mateusz Schabikowski[1,2], Alicja Cichoń[1,3], Zoltán Németh[4], Władysław Kubiak[3], Dariusz Kata[3] and Thomas Graule[1]

[1]Laboratory for High Performance Ceramics, Empa-Swiss Federal Laboratories for Materials Science and Technology, Switzerland

[2]Institute of Nuclear Physics, Polish Academy of Sciences, Poland

[3]Faculty of Materials Science and Ceramics, AGH University of Science and Technology, Poland

[4]Institute of Chemistry, University of Miskolc, Hungary

Keywords

sol-gel processes, fibers, transition metal oxides, biomedical applications

Abstract

This work describes the fabrication of ceramic fibres by electrospinning based on iron(III) oxide or copper(II) oxide. The fibres were produced from organic salt /polymer precursors and transformed into pure ceramic materials by firing. The fibres are aimed to remove negatively charged viruses from drinking water. The obtained ceramic fibres were characterised by the diameters of 0.23 ± 0.10 μm and 0.17 ± 0.06 μm for iron- and copper-based fibres, respectively. The performance of 0.100 g of fibres in the removal of MS2 bacteriophages in batch adsorption experiments reached the log reduction value (LRV) of 1.70 and 0.44 after 5 min and 10 minutes of contact time for iron(III) oxide and copper(II) oxide fibres, respectively.

Keywords

A. Sol-gel processes, B. Fibres, D. Transition metal oxides, E. Biomedical applications

1. Introduction

Despite the fact that the quality of life in the world does increase, there are still many regions suffering from the lack of access to basic services. Among them is the access to safe drinking water. According to the World Health Organization (WHO) [1], 844 million people lacked a basic drinking water service in 2015. The Sustainable Development Goal global target is to achieve a universal and equitable access to safe and affordable drinking water for all by 2030. WHO defines a basic drinking service as an access to drinking water from an improved source with the collection time not longer than 30 minutes for a round trip, including queuing. The point-of-use (POU) filters are devices providing on-site protection in the last possible moment before water use. Thus, the search for affordable and accessible materials for POU filters is still much in demand.

Iron(III) oxide in its hematite phase, α-Fe_2O_3, is a good choice for such materials. It was used to purify water from heavy metals and their compounds, such as arsenic [2] or chromate oxyanions [3]. It is inexpensive and widely available.

Copper(II) oxide, CuO, was the second material used in this research. It is known for its antibacterial [4, 5], antifungal [4] or antiviral [6] properties. Cu^{2+} ions were reported [7] to have had an impact on the conformation of specific peptides, which could potentially lead to an indirect destabilisation of some viruses. In the past, CuO was used as an additive or a modifier of various materials, e.g. fibres [8]. Gabbay and colleagues implemented it to impregnate socks and showed its antimicrobial and antifungal enhancement [4].

To apply the selected substances, we formed them into submicron fibres. Such a shape provides a large surface-to-volume ratio and allows to easily tailor the properties of the final product, such as the pore size or the porosity. Moreover, the fibres will separate the contaminants with the use of electrostatic adsorption [9] and not size exclusion.

There are numerous techniques to fabricate fibres of submicron dimensions. The most notable examples are electrospinning, melt blow spinning [10], rotary jet-spinning [11, 12] and forcespinning [13] are notable examples.

One of the first works on electrospinning was presented by Charles L. Norton in his patent in 1936 [14], in which he presented a method to form fibres from a viscous liquid capable to solidify rapidly. It was a step forward from electrospraying which had been developed earlier but produced strings of a liquid broken into droplets. Norton described the fibres formed in this way "*(…) well suited for packing, insulation, or similar purposes*.". He also emphasised that the contour of fibres could be changed into more irregular form by applying an external force. The force might have the form of an electric field or an air blast, perpendicular to the flow of the newly-formed liquid strings before their solidification. Thirty years later, Simons patented a method for the production of patterned non-woven fabrics by using electrospinning [15]. The difference between Norton's and Simons' work was , as Simons indicated, the possibility "*(…) for the spun fibres to be gathered into a thin, lightweight non-woven fabric with a pattern simulating any desired woven fabric (…)*".

Since then, electrospinning has evolved into a mature technique for the fabrication of fibres. This was especially visible when nanomaterials and nanofibres were and still are the main interest of many applications. Electrospun fibres are typically in the range of tens to hundreds of nanometers. Electrospun fibres are applied in many different fields of science and technology, such as photocatalysis [16], water purification [3, 17, 18], supercapacitors [19], batteries [20], cell growth [21–23], dielectric composites [24, 25], distillation [26] and others. This method is also considered the most common to fabricate nanofibres.

In our work, we used electrospinning to fabricate ceramic fibres based on iron or copper oxide from the mixture of the organic salts of metals and the polymer. After the formation of the filaments, the composite fibres were calcinated at various temperatures to transform the organic salts into their oxides and to remove the polymer from the fibres. Finally, the fibres were tested for their capability to remove MS2 bacteriophages which may be used as surrogates for negatively charged (in drinking water) human pathogenic viruses.

2. Material and methods

2.1. The precursors

The fabrication of the ceramic electrospun fibres was realised by dissolving 6.00 g of poly(N-vinyl-2-pyrrolidone) (PVP) of the molecular weight of 1300000 g/mol, obtained from Sigma-Aldrich (Switzerland), in 24.6 cm^3 of methanol under mechanical stirring at 250 rpm for at least 1 hour. Simultaneously, 0.60 g of $Fe(CH_3COO)_2$ (iron(II) acetate, 97%, ABCR GmbH & Co. KG, Germany; further denoted as "$Fe(Ac)_2$") or 0.06 g of $Cu(CH_3COO)_2$ (copper(II) acetate, 99% anhydrous, ACROS Organics^{TM}, Belgium; further denoted as "$Cu(Ac)_2$") was dissolved in 20.0 cm^3 of methanol with the addition of 0.01 cm^3 of CH_3COOH for the iron- and copper-based fibres, respectively. The amounts of the acetates were dictated by their solubility in methanol. The values represent approximately the maximal amounts soluble at room temperature with the practical duration of mechanical stirring. After the complete dissolution of the salts, the polymer solution was added to the salt solution. The mixture was magnetically stirred for an additional hour to ensure proper mixing of the two components. Each dissolution and mixing was conducted in a closed bottle to avoid losses of the volatile solvent.

The used acetic acid, CH_3COOH, and methanol, CH_3OH, were of a technical grade.

The precursors were analysed in terms of viscosity in the function of a shear rate. The measurements were performed at 25 °C with the use of the rotational viscosimeter Rheolab MC 120 (PhysicaMesstechnik GmbH, Germany). Each measurement consisted of increasing the shear rate from 10 to 2000 1/s and decreasing back to 10. Three such cycles were performed for each type of the precursors. The results are calculated mean values from the six slopes: three series with increasing shear rate and three with a decreasing one.

2.2. The spinning

The fibres were spun with the use of NEU-Pro device (Tong Li Tech Co. LTD, China) equipped with syringe pumps to feed the precursors of the fibres into a five-needle (of the inner diameter of 0.603 mm) head through a polypropylene tubing. The voltage was applied to the needles whereas the rotating drum was grounded.

The precursor was loaded into a 10 cm^3 plastic syringe connected to the electrospinning head. The solution was pumped at a constant rate of 0.5 cm^3/h. The collecting drum was covered with aluminum foil and sprayed with WD-40 lubricant to prevent the mats from sticking to its surface. The drum was then placed 16 cm from the spinneret head and set in motion (10 rpm). The voltage of 20 kV was applied to the spinneret. The measured ambient conditions in the spinning chamber were 24.5 °C and the humidity of 40%. As soon as the whole precursor was used, the fibres collected on the drum were gently removed from the foil.

2.3. MS2 Bacteriophages

In this study, MS2 bacteriophage was selected as a virus surrogate. MS2 is a commonly studied surrogate for human enteric viruses detected in drinking water [27-29]. This F-specific RNA bacteriophage is a member of the Leviviridae family. The phage consists of a 20 - 30 nm diameter proteic capsid and a 3566 nucleotides RNA genome partly bound to the capsid. The capsid exhibits pores on its surface and contains 180 copies of the capsid protein (13.7 kDa) and one copy of the maturation protein (44 kDa). The reported isoelectric point of MS2 is in the range of 2.2 - 3.9 [27, 28, 30]. The bacteriophages MS2 (DSMZ #13767) were obtained from the German Collection of Microorganisms and Cell Cultures (DSMZ, Germany).

2.4. The calcination

In order to transform the organic salts of the metals and to remove the fibre-forming polymer, the fibres were calcinated under oxidative atmosphere in the range of temperatures of 500 - 1000 °C with the constant heating and cooling rate of 1 °C/min. Such slow processing was selected to avoid unnecessary tension resulting from the rapid expansion of gases being the products of thermal decomposition of the salts.

The thermal decomposition of the acetate powders, as well as the composite fibres, was analysed with the use of thermogravimetry (TG). The measurements were conducted in Mettler Toledo TGA/sDTA 851e (Mettler Toledo, Switzerland) up to 1100 °C with the heating rate of 5 °C/min with a flowing air atmosphere using 150 mm^3 Al_2O_3 crucibles.

*2.5. The assessment of the properties of the fibres*The morphology of the fibres was observed by scanning electron microscopy (SEM) with the use of Vega TS 5130 (TeScan s.r.o., Czech Republic) and Nova NanoSEM 230 (FEI, USA) for high-resolution micrographs. Each specimen was coated with the conductive layer of Au-Pd with the use of Cressington 108auto Sputter Coater (Ted Pella Inc., USA) prior SEM observations. The diameters of the fibres were analysed from the SEM micrographs using ImageJ software (National Institutes of Health, USA). The average diameter was calculated from at least 100 measured fibres for each sample. The specific surface area of the fibres was determined according to the Brunauer-Emmett-Teller theory (BET) using Coulter SA3100 Surface Area and Pore Size Analyzer (Beckman-Coulter, USA). The samples were dried under flowing air at 180 °C for 1 hour prior to the measurements in Coulter SA-Prep Surface Area Outgas Station (Beckman-Coulter, USA).The zeta potential of the fibres was calculated from streaming potential measurements (according to the equation 1) by the Anton Paar software performed with SurPASS Electrokinetic Analyzer (Anton Paar GmbH, Austria) equipped with an integrated titration unit.

$$\zeta = \frac{dU}{dp} \cdot \frac{\eta}{\varepsilon \cdot \varepsilon_0} \cdot \frac{L}{A \cdot R} \quad (1)$$

where: ζ - zeta potential, dU/dp - the slope of streaming potential in the function of pressure, η - viscosity, ε - the dielectric constant of the electrolyte, ε_0 - electrical permittivity of vacuum, L - the length of the capillary system (the distance between the electrodes measuring the streaming potential in the system), A - the cross-sectional area of the capillary system, R - alternate current resistance of the dI capillary system filled with the electrolyte.

Ultrapure water, purified with Barnstead™ Nanopure™ (Thermo Scientific, USA), was used to prepare the electrolyte and to rinse the system. The electrolyte solution for the measurements was 0.001 M KCl. The titrants used to adjust pH were either 0.5 M NaOH or 0.5 M HCl. The sigmoidal fit for the zeta potential was performed with Fityk software [31].

2.6. The bacteriophage retention batch tests

The Fe_2O_3 and CuO electrospun fibres annealed at 500 °C were tested for the retention of MS2 bacteriophages. The batch adsorption was performed in a glass beaker containing 200 cm^3 of a virus dilution buffer (pH = 7.5). The liquid was monitored in terms of pH changes and constantly stirred at 350 rpm with the use of a magnetic stirrer. Next, 20 mm^3 of the self-propagated and purified MS2 bacteriophages (the concentration of $5 \cdot 10^6$ pfu/cm^3, plaque forming units per cubic centimetre) was added to the buffer and stirred for 5 minutes. After 5 minutes, 0.100 g of the electrospun fibres were added to the suspension. At this point, the sample of 1 cm^3 was taken every 5 minutes. The experiment was conducted for 30 minutes in total. After the sample was collected, it was filtered through a PTFE membrane (pore size = 5 μm) to physically remove possible bacterial contamination or bacterial cell debris originating fromthe lysis of bacteria. The membrane filtration and air exposure in the same conditions were experimentally confirmed [29] to have no statistically significant influence on the results.

Next, the amounts of MS2 bacteriophages in the collected samples were enumerated with the use of the double plate agar method [29, 32]. A collected sample (100 mm^3) containing MS2 was added to 200 mm^3 of Escherichia Coli (Migula 1895, Castellani and Chalmers 1919, DSM No.: 5695) suspension (Optical Density at 600 nm = 0.2). This mixture was then added to 7 cm^3 of liquid soft agar kept at 56 °C and homogenised. Next, the suspension was poured onto a hard agar plate and incubated at 37 °C for 24 hours. During this time, the bacteria grow and form a milky semi-transparent layer while active MS2 bacteriophages infect them. As a result, fully transparent spots in the bacterial layer appear and can be counted. Each spot represents a plague-forming unit of the bacteriophage.

The effectiveness of the MS2 removal was evaluated with the use of the Log Reduction Value (LRV) which was calculated from the equation 2

$$LRV_i = -\log_{10}(1-R_i) \qquad (2)$$

where: LRV_i - the Log Reduction Value, R_i - the retention of the bacteriophages which was calculated according to the equation 3

$$R_i = 1 - \frac{C_i}{C_{i0}} \quad (3)$$

where: C_i - the concentration of the bacteriophages after purification, C_{i0} - the initial concentration of the bacteriophages. The LRV of 1 corresponds to the tenfold decrease of the concentration of the relevant species.

3. Results and discussion

3.1. The rheology of the fibre precursors

The viscosity relation of the iron- and copper-based precursors is presented in Figure 1. The polymer exhibits the shear thinning effect resulting in the decrease of its viscosity with an increasing shear rate.

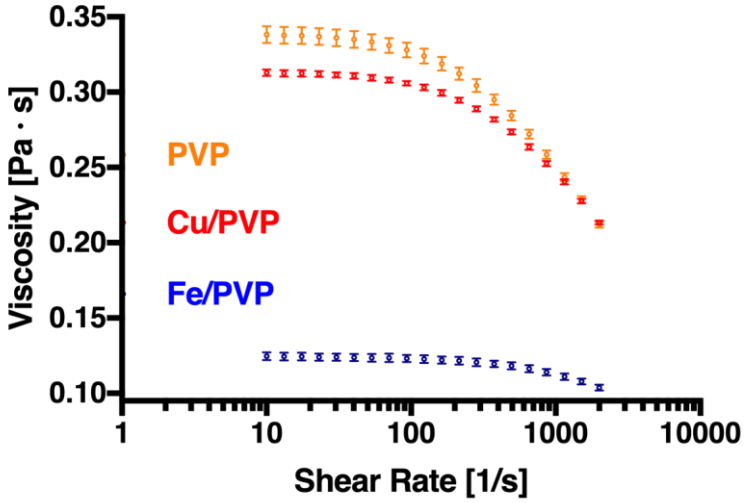

Figure 1. The viscosity of the fibre precursors in the function of a shear rate.

Such behaviour is beneficial in the systems in which a viscous liquid is pumped through conduits, such as presented electrospinning system. The addition of the copper salt resulted in the decrease of 0.025 Pa · s for the lowest shear rates (10 1/s). Presumably, this reduction is caused by the distortion of PVP chains arrangement. The relatively long chains (1300000 g/mol) of the polymer create a mesh with hydrogen bonds formed between them. This mesh is destroyed with increasing stirring forces which explains the decrease in viscosity at the higher shear rate of the rheometer. The formation of the bonds, as well as the layout of the chains, are distorted by the introduction of additional molecules of the metallic salts. At a higher shear rate, the distortion caused by the stirring forces becomes dominant and the viscosity equalises with the viscosity of the PVP solution.

The introduction of $Fe(Ac)_2$ also leads to the reduction of the viscosity which is approximately 8.6 times higher than that caused by $Cu(Ac)_2$ (0.214 Pa · s and 0.025 Pa · s, respectively). Since we introduced 10.5 times more mols of $Fe(Ac)_2$, we assume the difference of 8.6 times in the decrease of the viscosity derives from the larger amount of the iron salt. However, this hypothesis was not further investigated.

3.2. The morphology of the composite fibres

The morphology of the electrospun polymer/ceramic fibres is presented in Figure 2. The obtained fibres formed mats consisting of randomly oriented non-woven filaments.

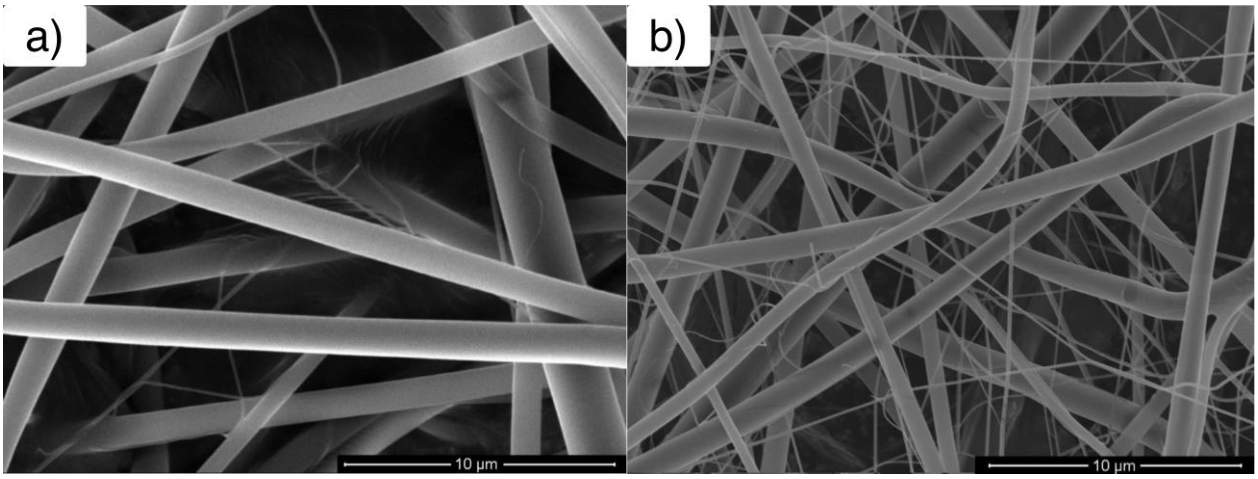

Figure 2. The morphology of the electrospun composite fibres: a) copper-based, b) iron-based.

The fibres were of a cylindrical shape with no visible open porosity. The surface of the fibres was smooth and without major defects. No solidified droplets formed due to the breakage of liquid jets were observed. Both types of fibres consisted of a mixture of fibres of different fineness with copper-based fibres having their diameter less homogeneous (as will be shown in Figure 6). The larger size of the copper-based fibres is mainly related to the higher viscosity of their precursor in comparison to the iron-based precursor.

3.3. The thermogravimetric analysis

To select the appropriate temperature for the removal of PVP and the transformation of the organic salts into oxides, thermogravimetric measurements were performed (Figure 3).

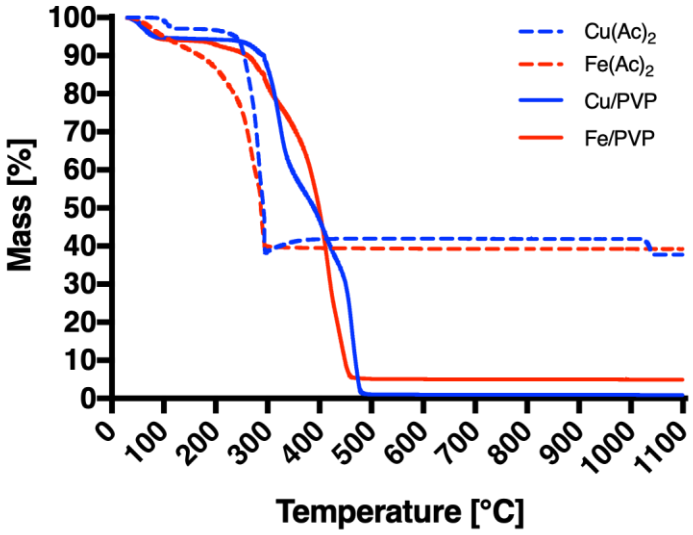

Figure 3. The thermogravimetric analysis of the precursor powders and electrospun composite fibres.

The mass of $Cu(Ac)_2$ starts to rapidly decline at approximately 270 °C indicating the thermal decomposition of the salt. Next, it reaches the minimum of 39.7% at 316.2 °C. Later, it increases gently to the plateau at approximately 41.9% until 1016 °C where we observed another decline. The calculated mass percentage of copper(II) oxide to the mass of copper(II) acetate equals 43.8%. The difference between the obtained and the calculated percentage may result from the used base material (the purity of 99%) and the formation of other oxides such as copper(I) oxide.

The thermal decomposition of $Fe(Ac)_2$ occurs in a broader range of temperatures with the elevated decline starting already at approximately 120 °C. The mass reaches the minimum of approximately 39.7% at the same temperature as $Cu(Ac)_2$, 316.2 °C. Thus, we assume this is the temperature where the majority of the mass and the mutual part of both salts finish its decomposition. The calculated mass percentage of Fe_2O_3 of the two $Fe(Ac)_2$ is 45.9%. The larger difference between the calculated mass of the oxide and the experimentally evaluated mass may possibly derive from the lower purity of the iron(II) acetate (97%) and the formation of other oxides such as iron(II, III) oxide, Fe_3O_4.

The thermogravimetric analysis of the electrospun fibres shows a much larger weight loss compared to the salts. The mass reaches 1.0 % and 5.2 % of its starting mass at 502.9 °C and 487.2 °C and keeps this level at higher temperatures (copper- and iron-based fibres, respectively). These characteristics are close to the thermal properties of PVP which is understandable because of the used mass proportions. Huang and others [33] reported the residual mass of PVP (Mw = 360000 g/mol) at 4 % at the temperature 430.5 °C. In this work, a PVP of a larger molecular weight was used (1300000 g/mol) which explains the difference. Copper-based fibres contain less salt comparing to the iron-based fibres, yet the latter is closer to the thermal characteristics of PVP. This phenomenon was not further investigated.

3.4. The morphology of the calcinated fibres

The calcinated copper-based fibres are presented in Figure 4. The heat treatment at 500 °C and the removal of the polymer resulted in the fibres becoming shorter, thinner and jagged on the edges (Figure 4a).

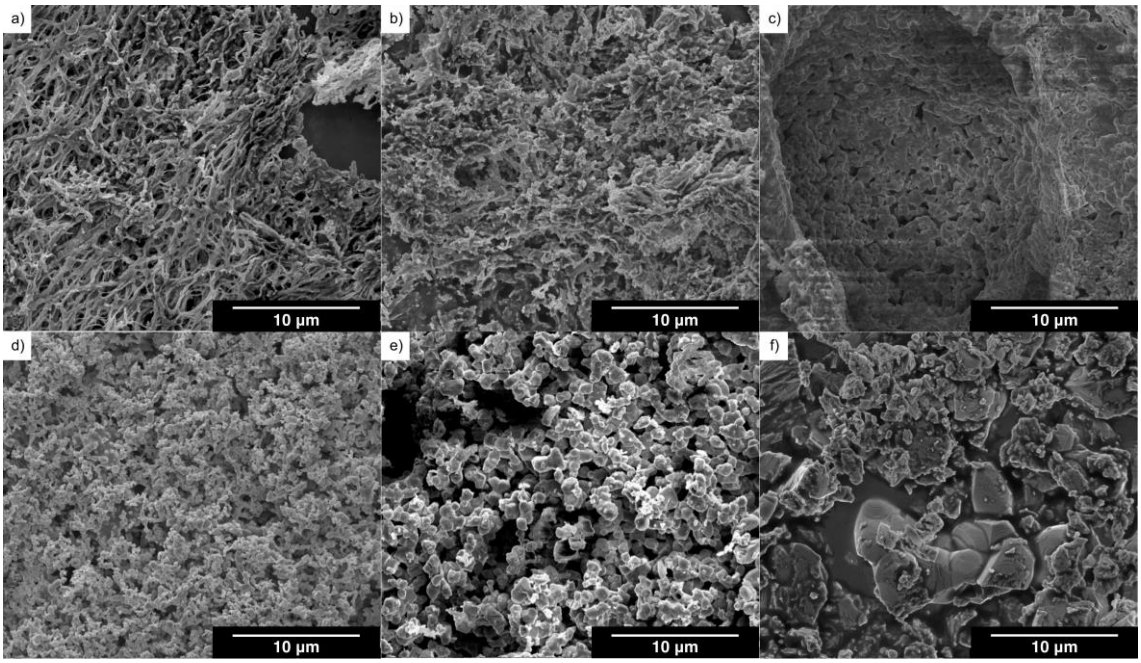

Figure 4. The morphology of the calcinated copper-based fibres: a) 500 °C, b) 600°C, c) 700°C, d) 800°C, e) 900 °C, f) 1000 °C.

The filaments formed a connected mesh with the occasional formation of solid areas. The membranes contained numerous open pores. The calcination at 600 °C transformed the fibres into a more compact material with little to none indistinguishable separate filaments. The fibres formed cauliflower-like structures with, presumably, decreased porosity in comparison to fibres calcinated at 500 °C (based on the assessment of the optical qualitative analysis of SEM micrographs). The heat treatment at 700 °C practically disintegrated the oblong leftovers of the fibres. The material took the form of almost completely molten grains with significantly decreased open porosity. The transition from 700 °C to 800 °C led to the crystallisation of agglomerated nanoparticles with considerably increased crystallinity (as will be shown in Figure 7a). From this point, the grains grew in size with the increasing temperature of the heat treatment.

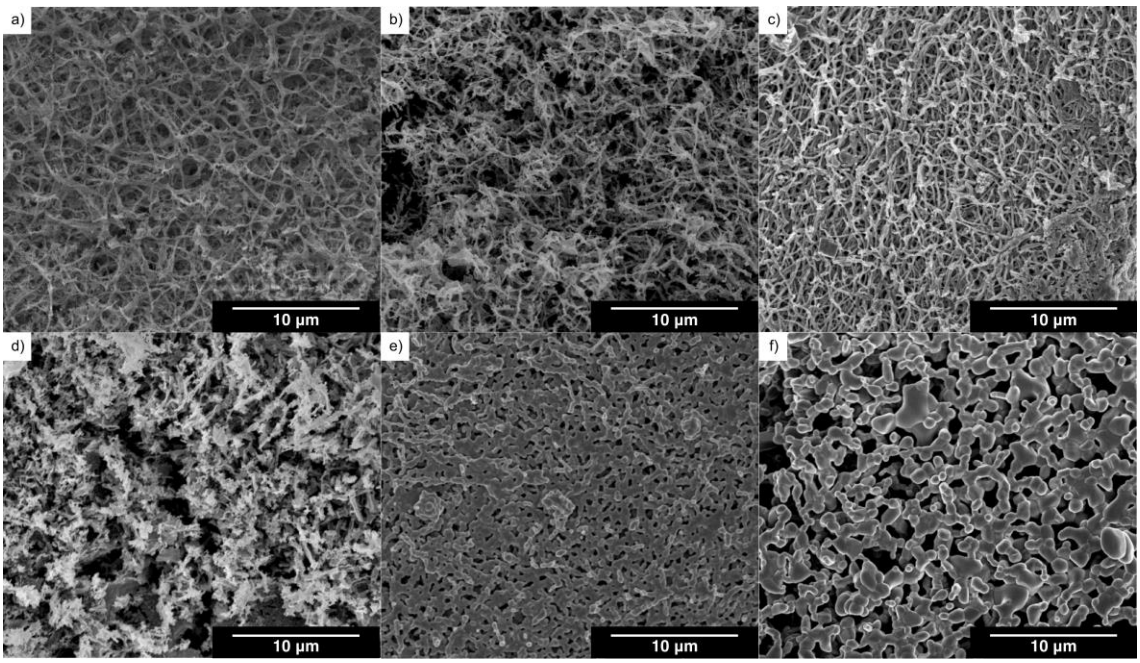

Figure 5. The morphology of calcinated iron-based fibres: a) 500 °C, b) 600°C, c) 700°C, d) 800°C, e) 900 °C, f) 1000 °C.

The iron-based fibres annealed at 500 °C formed a looser mesh of fibres compared to the copper-based fibres (Figure 5). In certain areas, web-like surfaces connecting several filaments were formed. Heating at 600 °C lead to the breakage of the fibres and resulted in substantial shortening of their length. The interconnecting porous layer (the web-like structures) was still present in the material. A further increase of the temperature caused the smaller fibres to melt and form thickenings on the larger fibres (visible as bright regions in Figure 5c).Heating at 800 °C destroyed the mesh of fibres and dramatically shortened their length. The material was in the form of a separated island with needle-like structures. The annealing at 900 °C and 1000 °C caused the material to melt (Figure 5e, f). The separated needles coalesced into a worm-like shape which further enlarged at the highest temperature.

As the focus of this study was on a fibrous material, the fibres calcinated at 500 °C were selected for further analyses of base materials.

The specific surface area of the fibres annealed at 500 °C was evaluated according to BET. The iron-based fibres were characterised by the specific surface area of 17.12 m^2/g. For the copper-based fibres, the value decreased to 3.24 m^2/g which correlates well with the results of the analysis of the size of the fibres.

3.5. The diameter distributions

The diameters of electrospun composite fibreswere not homogeneous. They were characterised by a bi- and tri-modal size distribution for Cu/PVP and Fe/PVP, respectively (Figure 6).

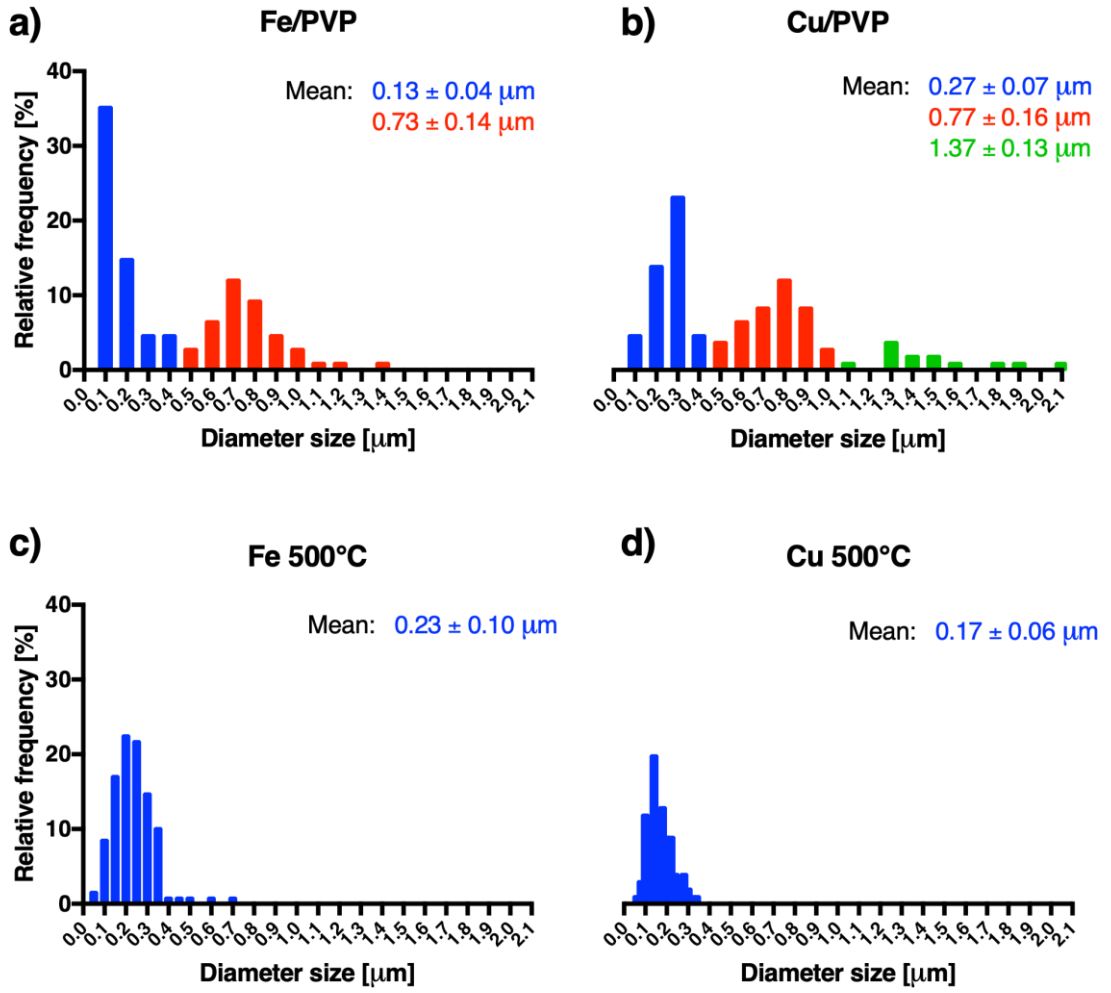

Figure 6. The diameter distribution of the electrospun fibres: a) iron-based composite fibres, b) copper-based composite fibres, c) iron-based fibres calcinated at 500 °C, d) copper-based fibres calcinated at 500 °C.

Each interval of the diameters was colour coded for better illustration. Iron-based fibres were characterised by the smallest size distribution with the average of 0.13 ± 0.04 µm. The smallest batch of Cu/PVP was of almost twice the size of Fe/PVP with the average of 0.27 ± 0.07 µm. The second interval of the sizes reached 0.73 ± 0.14 µm and 0.77 ± 0.16 µm for Fe/PVP and Cu/PVP, respectively, which makes them very similar for both materials. The third and the largest interval of the sizes was present only for the copper-based fibres and reached 1.37 ± 0.13 µm.

To summarise, the Fe/PVP was more homogeneous and of a smaller size in comparison to Cu/PVP. One of the factors dictating such behaviour might be the larger viscosity of the copper-based precursor which normally results in the increase of the fibre size.

The heat treatment at 500 °C substantially reduced the size of both types of fibres as expected. The greatest influence on this effect was the removal of PVP but the transition from the organic salts into oxides did influence that as well. The calcinated fibres exhibit a unimodal distribution of the diameters in both cases. The average size of the diameters were 0.23 ± 0.10 µm and 0.17 ± 0.06 µm for the iron and copper-based fibres, respectively. Both types of fibres were of a similar size on average despite the tenfold difference of the salt content (from the weight point of view, the iron-based precursors contained ten times more salt than the copper-based ones).

3.6. The phase composition of the calcinated fibres

The annealed copper-based fibres consisted mainly of tenorite (CuO, reference code: 00-045-0937) with the small amount of the partially oxidised cuprite (Cu_2O, reference code: 00-005-0667) phase (Figure 7a). The relatively low intensity of the reflections at temperatures lower than 800 °C suggests a moderately unordered structure of the formed oxides. A large increase in the intensity of the X-ray diffraction signal upon reaching 800 °C was observed. The increased intensity was persistent in the higher temperatures. The two most intense reflections changed ratio at 900 °C and 1000 °C in comparison to the ratios observed at lower temperatures. However, this behaviour was not investigated since the suitable morphology was obtained already at 500 °C.

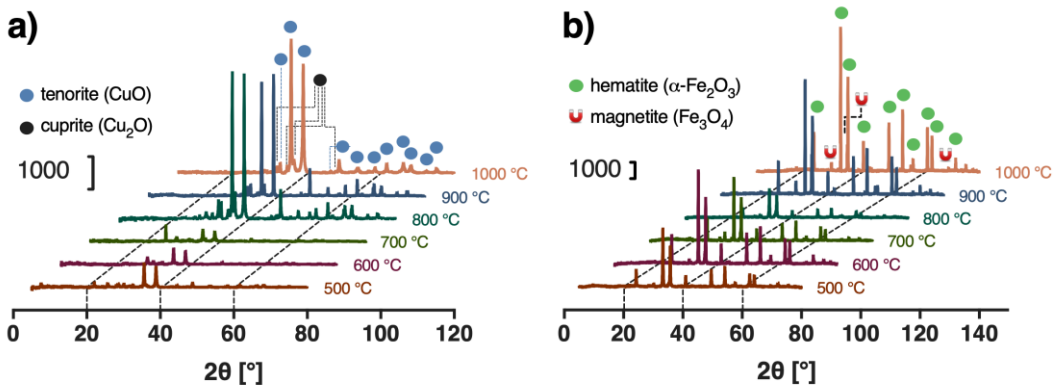

Figure 7. The phase composition of the annealed fibres: a) copper-based, b) iron-based.

The diffractograms of the annealed iron-based fibres reveal that hematite (α-Fe_2O_3, reference codes of the used XRD patterns: 00-001-1053, 00-013-0534) is their main constituent (Figure 7b). The small-intensity reflections of magnetite (Fe_3O_4, reference code: 00-019-0629) are also present in the whole range of annealing temperatures. Their intensity changes proportionally to the intensity of the strongest reflections after each heat treatment.The list of the detected reflections for the materials after calcination at 500 °C is shown in Supplementary Material 1.

3.7. The electrokinetic properties of the iron-based fibres

The zeta potential was measured for the iron-based fibres annealed at 500 °C. Due to the technical difficulties with the apparatus (leaking tubing), only the annealed iron-based fibres could be measured. The isoelectric point of the fibres was equal to 8.9 and was calculated from the sigmoid function fit (Figure 8).

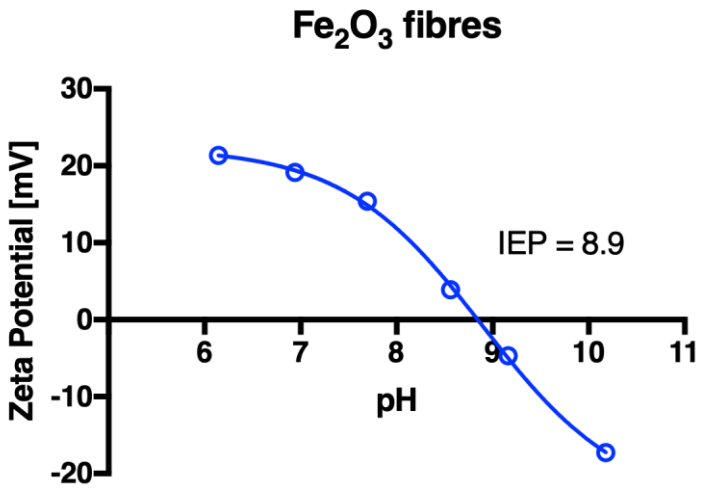

Figure 8. The electrokinetic properties of the annealed iron-based fibres.

The obtained result is in close agreement with the values reported in the literature for α-Fe_2O_3, such as 8.5 reported by Park [34] or 9.3 by Kittaka and others [35]. Such electrokinetic properties are beneficial for the adsorption of MS2 bacteriophages since their isoelectric point is in the range of 2.2 - 3.9 [30]. Thus electrostatic attraction between them is formed. It is the principle of electrostatically enhanced adsorption often utilised in water purification techniques.

The isoelectric point of CuO is expected to be in the range of 9.1 - 9.7 with a calculated value of 9.3 [36]. However, the surface properties depend on many parameters such as the history of the sample, preparation (thus a manufacturer), etc, and as low values as 6.7 were also reported [8].

3.8. The MS2 removal of the ceramic fibres

The results of the MS2 removal experiments are illustrated in Figure 9. The fibres based on hematite were considerably more effective in removing or inactivating (since the test validate the number of active phages, we cannot specify it precisely) the bacteriophages. The largest log reduction values (LRV) were achieved practically immediately after the addition of the fibres to the suspension. The LRV in later stages remained at the same level within the statistical error of the enumeration method. The obtained maximal values of LRV were 1.70 and 0.44 for the iron- and copper-based fibres, respectively.

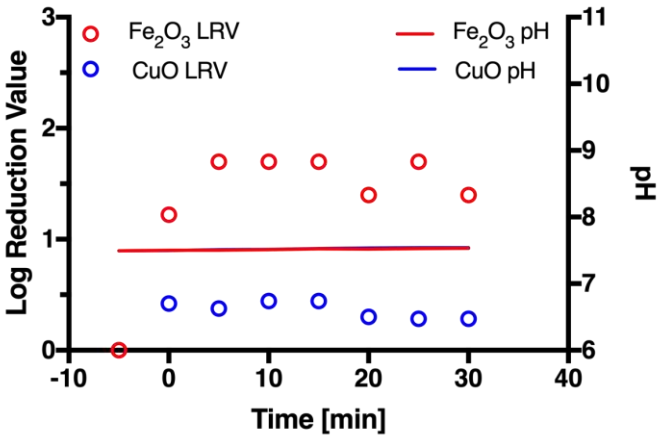

Figure 9. The removal of MS2 bacteriophages by the electrospun fibres in batch experiments.

One of the advantages of the hematite fibres over the copper-based fibres was their superior specific surface area. This parameter plays one of the most important roles in adsorption. With the larger specific surface area and small size, the iron-based fibres provided more adsorption sites and contact area to the surrounding water with MS2 bacteriophages.

Both types of fibres did not remove all applied bacteriophages. However, the results are promising especially for the iron-based fibres. To compare, Borkov and others achieved the LRV between 0.74 and 4.6 depending on the tested virus types with their copper oxide-impregnated polypropylene fibres [6]. Boudaud and others reported the removal of MS2 at the LRV of above or equal 4.0 with the use of a conventional drinking water treatment at a pilot scale [27]. However, that treatment is a complex multistep process involving coagulation, flocculation, lamellar settling, sand filtration and a membrane ultrafiltration process. Hongyang and others achieved the retention of approximately LRV 2.0 with the use of their electrospun functionalised polymeric membrane and reported the efficiency of approximately LRV of 1.0 of the GS0.22 commercial membranes [18]. Using an impregnated cellulose fibres with metallic copper, Szekeres and others [29] achieved the retention of at least LRV = 5 (the limit of their experiment) at three pH values. The authors used the cellulose fibres as a structural material with impregnated MS2-inactivating copper. This work shows the results of an active materials to adsorb the bacteriophages which, with its further implementation in a filter, can potentially achieve similar performance.

4. Conclusions

The electrospun fibres after the heat treatment transformed into ceramic oxide-based materials of a submicron diameter. As expected, this transition occurred with a significant decrease of the diameters of the fibres. The treatment at 500°C produced fibres of the most beneficial morphology. The iron-based fibres were superior to the copper-based ones in terms of MS2 bacteriophage removal. The results were insufficient for drinking water purification. However, they are promising since they were obtained in batch experiments where the adsorbents and adsorbates have to travel to each other. Building a filter based on the membrane made of the fibres should significantly increase the performance. Moreover, the adsorption does not rely on the size exclusion, hence the membranes need not be as tightly packed as in the case of size-exclusion membranes (though a good contact of the adsorbates to the medium must be preserved). This would improve the flow of a filtrate and pressure drop on the filter. Finally, the fibres are purely ceramic so it is possible to clean them conventionally by firing.

5. Acknowledgements

The authors are grateful to Dr. Tony Lusiola for the aid and consultations concerning the preparations of the fibre precursors.

Funding: This work was supported by Switzerland through the Swiss Contribution to the enlarged European Union within the project "Novel nanocomposite filter media for adsorption based water treatment NANOSORP", PSRP: 209/2010.

6. Bibliography

1. Organization WH, Fund TUNC. Progress on Drinking Water, Sanitation and Hygiene: 2017 update and SDG baselines. 2017

2. Zaspalis V, Pagana A, Sklari S. Arsenic removal from contaminated water by iron oxide sorbents and porous ceramic membranes. Desalination 2007; 217: 167-180

3. Peter KT, Johns AJ, Myung NV et al. Functionalized polymer-iron oxide hybrid nanofibers: Electrospun filtration devices for metal oxyanion removal. *Water Res* 2017; 117: 207-217

4. Gabbay J, Borkow G, Mishal J et al. Copper oxide impregnated textiles with potent biocidal activities. *J Ind Text* 2006; 35: 323-335

5. Ren G, Hu D, Cheng EWC et al. Characterisation of copper oxide nanoparticles for antimicrobial applications. *Int J Antimicrob Agents* 2009; 33: 587-590

6. Borkow G, Sidwell RW, Smee DF et al. Neutralizing viruses in suspensions by copper oxide-based filters. *Antimicrob Agents Chemother* 2007; 51: 2605-2607

7. Uber D, Wyrzykowski D, Tiberi C et al. Conformation-dependent affinity of Cu(II) ions peptide complexes derived from the human Pin1 protein: ITC and DSC study. *J Therm Anal Calorim* 2017; 127: 1431-1443

8. Schabikowski M, Zalewska M, Kata D et al. The effect of CuO coatings on the electrokinetic properties of stone wool fibres determined by streaming potential measurements. *Ceram Int* 2016; 42: 13944-13951

9. Schabikowski M, Niżnik A, Kata D et al. The adsorption of polystyrene nanoparticles on selected commercially available fibers: a streaming potential study. *Text Res J* 2017; 004051751773208

10. Podgórski A, Bałazy A, Gradoń L. Application of nanofibers to improve the filtration efficiency of the most penetrating aerosol particles in fibrous filters. *Chem Eng Sci* 2006; 61: 6804-6815

11. Badrossamay MR, McIlwee HA, Goss JA et al. Nanofiber assembly by rotary jet-spinning. *Nano Lett* 2010; 10: 2257-2261

12. Schabikowski M, Tomaszewska J, Kata D et al. Rotary jet-spinning of hematite fibers. *Text Res J* 2014; 85: 316-324

13. Sarkar K, Gomez C, Zambrano S et al. Electrospinning to forcespinning™. *Mater Today* 2010; 13: 12-14

14. Norton CL. *Method of and apparatus for producing fibrous or filamentary material*. Patent US2048651, USA, 1936

15. Simons HL. *Process and apparatus for producing patterned non-woven fabrics.* Patent US3280229, USA, 1966

16. Sheikh FA, Appiah-Ntiamoah R, Zargar AM et al. Photocatalytic properties of Fe2O3-modified rutile TiO2 nanofibers formed by electrospinning technique. *Mater Chem Phys* 2015; 172: 62-68

17. Mahapatra A, Mishra BG, Hota G. Electrospun Fe2O3-Al2O3 nanocomposite fibers as efficient adsorbent for removal of heavy metal ions from aqueous solution. *J Hazard Mater* 2013; 258-259: 116-123

18. Ma H, Hsiao BS, Chu B. Functionalized electrospun nanofibrous microfiltration membranes for removal of bacteria and viruses. *J Membr Sci* 2014; 452: 446-452

19. Binitha G, Soumya MS, Madhavan AA et al. Electrospun α-Fe 2 O 3 nanostructures for supercapacitor applications. *J Mater Chem* A 2013; 1: 11698-11704

20. Wang L, Yu Y, Chen PC et al. Electrospinning synthesis of C/Fe3O4 composite nanofibers and their application for high performance lithium-ion batteries. *J Power Sources* 2008; 183: 717-723

21. Stachewicz U, Szewczyk PK, Kruk A et al. Pore shape and size dependence on cell growth into electrospun fiber scaffolds for tissue engineering: 2D and 3D analyses using SEM and FIB-SEM tomography. *Mater Sci Eng C* 2017;

22. Stachewicz U, Qiao T, Rawlinson SCF et al. 3D imaging of cell interactions with electrospun PLGA nanofiber membranes for bone regeneration. *Acta Biomater* 2015; 27: 88-100

23. Nandakumar A, Fernandes H, de Boer J et al. Fabrication of Bioactive Composite Scaffolds by Electrospinning for Bone Regeneration. *Macromol Biosci* 2010; 10: 1365-1373

24. Mohammadi M, Alizadeh P, Clemens FJ. Effect of using different precursors on electrospinning of CaCu3Ti4O12. *Ceram Int* 2016; 42: 4690-4699

25. Mohammadi M, Alizadeh P, Clemens FJ. Synthesis of CaCu3Ti4O12 nanofibers by electrospinning. *Ceram Int* 2015; 41: 13417-13424

26. Zhu Z, Liu Y, Hou H et al. Dual-Bioinspired Design for Constructing Membranes with Superhydrophobicity for Direct Contact Membrane Distillation. *Environ Sci Technol* 2018; 52: 3027-3036

27. Boudaud N, Machinal C, David F et al. Removal of MS2, Qβ and GA bacteriophages during drinking water treatment at pilot scale. *Water Res* 2012; 46: 2651-2664

28. Dowd SE, Pillai SD, Wang S et al. Delineating the specific influence of virus isoelectric point and size on virus adsorption and transport through sandy soils. *Appl Environ Microb* 1998; 64: 405-410

29. Szekeres GP, Németh Z, Schrantz K et al. Copper-Coated Cellulose-Based Water Filters for Virus Retention. *ACS Omega* 2018; 3: 446-454

30. Michen B, Graule T. Isoelectric points of viruses. *J Appl Microbiol* 2010; 109: 388-397

31. Wojdyr M. Fityk: a general-purpose peak fitting program. *J Appl Crystallogr* 2010; 43: 1126-1128

32. Moce-Llivina L, Lucena F, Jofre J. Double-Layer Plaque Assay for Quantification of Enteroviruses. *Applied and Environmental Microbiology* 2004; 70: 2801-2805

33. Huang S, Zhou L, Li MC et al. Preparation and Properties of Electrospun Poly (Vinyl Pyrrolidone)/Cellulose Nanocrystal/Silver Nanoparticle Composite Fibers. Materials (Basel) 2016; 9

34. Parks GA, de Bruyn PL. The Zero Point of Charge of Oxides. *J Phys Chem* 1962; 66: 967-973

35. Kittaka S. Isoelectric point of Al2O3, Cr2O3 and Fe2O3. I. Effect of heat treatment. *J Colloid Interf Sci* 1974; 48: 327-333

36. Kittaka S, Morimoto T. Isoelectric point of metal oxides and binary metal oxides having spinel structure. *J Colloid Interf Sci* 1980; 75: 398-403